
LAte: Hyperbolic Lorentz Attention for Cross-Subject EEG Classification

Johannes Burchert^{*1} Ahmad Bdeir^{*2} Tom Hanika¹ Lars Schmidt-Thieme¹ Niels Landwehr²

Abstract

Electroencephalogram (EEG) classification is critical for applications ranging from medical diagnostics to brain-computer interfaces, yet it remains challenging due to the inherently low signal-to-noise ratio (SNR) and high inter-subject variability. To address these issues, we propose LAte, a novel framework that integrates a Lorentz Attention Module with an InceptionTime-based encoder to enable robust and generalizable EEG classification. Unlike prior work, which evaluates primarily on single-subject performance, LAte focuses on cross-subject training. First, we learn a shared baseline signal across all subjects using pretraining tasks to capture common underlying patterns. Then, we utilize novel Lorentz low-rank adapters to learn subject-specific embeddings that model individual differences. This allows us to learn a shared model that performs robustly across subjects, and can be subsequently finetuned for individual subjects or used to generalize to unseen subjects. We evaluate LAte on three well-established EEG datasets, achieving a substantial improvement in performance over current state-of-the-art methods.

1. Introduction

Electroencephalogram (EEG) classification is an important task in time-series analysis from both a theoretical and a practical perspective. The problem is inherently complex and faces significant challenges (Parbat & Chakraborty, 2021; Pan et al., 2022), notably, EEG sequences are often contaminated with various artifacts, including eye blinks, eye movements, and muscle activity (Kotte & Dabbakuti, 2020; Delorme, 2023). These can significantly degrade the

quality of the recorded data and have diverse effects that obscure relevant neural signals. For example, ocular artifacts, including eye movements and blinks, produce large voltage fluctuations (Croft & Barry, 2000). Myogenic artifacts (Muthukumaraswamy, 2013; Pion-Tonachini et al., 2019), caused by facial and scalp muscle movements, introduce high-frequency noise that overlaps with the frequency bands of the brain signals. This reduces the signal-to-noise ratio and hinders the performance of downstream applications such as classification and clinical analysis.

To address these issues, previous approaches to EEG classification have explored geometric methods (Lotte et al., 2007), and deep learning techniques (Roy et al., 2019). In their work (Pan et al., 2022) introduces the Manifold Attention network (MAtt) which models the EEG data embeddings as symmetric positive-definite (SPD) matrices on a Riemannian manifold. They argue that Riemannian metrics are less sensitive to outliers and noise. More recently, Bdeir et al. (2025) introduced HyperMAtt, which extends the MAtt formulation by replacing the SPD operations in the decoder with Lorentzian equivalents. Our work takes this a step further by developing a fully hyperbolic model that leverages the unique geometry in both the encoder and the decoder.

Hyperbolic manifolds are naturally suited for representing hierarchical structures, a property that is extensively focused on in the Graph Neural Network literature (Mettes et al., 2024). At the same time, EEG data inherently exhibits spatial hierarchies from sensor arrangements and node signal interactions. This makes EEG classification settings potentially appropriate for hyperbolic learning. By capturing these hierarchies and modeling signal interactions directly in the Lorentz space, our approach learns more expressive latent representations and achieves good cross-subject generalization without requiring a separate model for each patient. To achieve this, we introduce several novel components such as the hyperbolic inception block and Lorentzian boost-based low-rank adapters (LoRAs) (Hu et al., 2022). Specifically, the latter component is able to inject subject-specific data patterns through unique ID embeddings. Additionally, we combat overfitting in data-sparse problems through self-supervised pretraining methods and random classifier projections. This allows us to extract global EEG features while explicitly distinguishing between subject-specific distributions, resulting in improved general-

¹ISMLL, University of Hildesheim, Hildesheim, Germany ²Data Science Group, University of Hildesheim, Hildesheim, Germany. Correspondence to: Johannes Burchert <burchert@ismll.de>, Ahmad Bdeir <bdeira@uni-hildesheim.de>, Tom Hanika <hanika@ismll.de>, Lars Schmidt-Thieme <schmidt-thieme@ismll.de>, Niels Landwehr <landwehr@uni-hildesheim.de>.

ization and adaptability to new subjects without retraining the model from scratch.

Our contributions in this paper are then focused on two key issues in the domain of EEG Classification, namely cross-subject training and generalization, and regularization for noisy input distributions:

1. We propose LAtte, a fully hyperbolic model for EEG Classification based on Lorentzian InceptionTime and attention blocks.
2. We propose a protocol for fine-tuning EEG models based on cross-subject training with subject-specific low-rank adapters.
3. We combat overfitting and data sparsity with a hyperbolic random projection classifier and self-supervised pre-training
4. We demonstrate the efficacy of LAtte on three well-established datasets in the domain of EEG classification. Here, we achieve an average improvement of 3.93% in the subject-specific and 10.73% in the subject-conditional setting over the state-of-the-art.

2. Related Work

EEG Classification Deep learning for EEG classification has been largely dominated by convolutional architectures that exploit the spatio-temporal structure of neural signals. CNN models such as EEGNet (Lawhern et al., 2018) and ShallowConvNet (Schirrneister et al., 2017) introduced lightweight pipelines combining temporal filtering with channel-wise spatial projections. Subsequent work refined this paradigm to better capture spatio-spectral structure, including SCCNet (Wei et al., 2019) and FBCNet (Mane et al., 2021), as well as temporally focused models such as EEG-TCNet (Ingolfsson et al., 2020) and TCNet-Fusion (Musallam et al., 2021). While effective, these methods remain Euclidean and are typically optimized in subject-specific settings with one model being trained per subject.

More recent approaches incorporate attention mechanisms and non-Euclidean geometry. MBEEGSE (Altuwaijri et al., 2022) integrates transformer-style attention with EEG-specific convolutions, and MAtt (Pan et al., 2022) operates on SPD manifolds to improve robustness to noise. These works suggest the promise of geometric representations, but still rely on predominantly Euclidean encoders and do not explicitly target cross-subject generalization.

Cross-subject EEG classification remains relatively under-explored outside of emotion recognition. Existing efforts include feature analyses (Li et al., 2018), meta-learning and contrastive objectives (Shen et al., 2023), pretraining (Cimtay & Ekmekcioglu, 2020), and transfer learning (Li

et al., 2020). More recently, Burchert et al. (2024) adapted time-series backbones such as ResNet and InceptionTime in a subject-dependent setting and TCFormer (Altaheri et al., 2025) evaluated a leave-one-subject-out protocol (Kunjan et al., 2021). Although these studies demonstrate the feasibility of joint training, they primarily rely on shallow encodings of subject-specific features.

In parallel, large-scale EEG foundation models such as LaBraM (Jiang et al., 2024) and CBraMod (Wang et al., 2025) learn universal EEG representations from large corpora such as Obeid & Picone (2016). However, they are not tailored to short sequence lengths due to fixed patch sizes of the pertaining process.

Unlike prior cross-subject methods that treat subject identity as auxiliary input, we parameterize subject-specific variation through low-rank adapters, enabling a single shared model to explicitly capture subject-specific distribution shifts. Our approach unifies hyperbolic representations and cross-subject learning within one framework.

Hyperbolic Learning Hyperbolic distance metrics scale exponentially with the distance to the origin. This allowed hyperbolic spaces higher embedding capacities and conformity with tree-like data relationships (Ganea et al., 2018). Early developments in hyperbolic deep learning frequently adopted hybrid architectures that paired Euclidean encoders with hyperbolic decoders (Mettes et al., 2024). This design choice mitigated the computational overhead associated with hyperbolic operations and circumvented the absence of well-established hyperbolic analogues for many standard Euclidean components. However, recent work has increasingly shifted towards fully hyperbolic models to better exploit the geometric inductive biases of hyperbolic space.

Chen et al. (2022) advanced this direction by introducing hyperbolic counterparts to several foundational components, including fully connected layers, graph convolution layers, and the attention mechanisms. Specifically, their architecture employs the square Lorentzian distance as a similarity metric and learns class prototypes directly in hyperbolic space. They build on earlier works such as Atigh et al. (2022), Kim et al. (2023), and Mettes et al. (2024) by directly replacing the loss with this distance metric.

This approach was later extended to EEG tasks, most notably in the works of Nguyen et al. (2025) and Bdeir et al. (2025). Nguyen et al. (2025) proposed a unified framework for neural networks on symmetric spaces of noncompact type, which include both hyperbolic and SPD manifolds. Their approach is built around a generalized formulation of the point-to-hyperplane distance and derives closed-form expressions to construct hyperbolic fully connected layers and attention mechanisms. In parallel, Bdeir et al. (2025) introduced HyperMatt, an extension of the Matt framework

(Pan et al., 2022) that replaces the original SPD decoder with a Lorentz-based hyperbolic decoder. Specifically, they project the SPD matrices on the Lorentz space and apply Lorentzian attention and a hyperbolic MLR as a final classification layer. Although this represents an important step toward leveraging hyperbolic geometry for EEG, the encoder remains non-hyperbolic. As a result, there may still be possible performance gains from fully capturing the hierarchical relationships inherent in EEG data.

3. Background

Lorentz Manifold Hyperbolic space is a Riemannian manifold characterized by constant negative sectional curvature $-1/K < 0$ where K is the curvature surrogate. In the following work, we adopt the Lorentz model of hyperbolic space (also known as the hyperboloid model), which uses the upper sheet of a two-sheeted hyperboloid within Minkowski space. The n -dimensional Lorentz space is then defined as $\mathbb{L}_K^n = (\mathcal{L}^n, \mathfrak{g}_x)$, where the manifold \mathcal{L}^n is

$$\mathcal{L}^n := \{ \mathbf{x} = [x_t, \mathbf{x}_s] \in \mathbb{R}^{n+1} \mid \langle \mathbf{x}, \mathbf{x} \rangle_{\mathcal{L}} = -K, x_t > 0 \},$$

The Lorentzian inner product defines the Riemannian metric $\langle \mathbf{x}, \mathbf{y} \rangle_{\mathcal{L}} := -x_t y_t + \mathbf{x}_s^\top \mathbf{y}_s$. Following terminology from special relativity, we refer to x_t as the *time* component and \mathbf{x}_s as the *space* component. We can then use the definition of the inner product and the terminology to define the origin of the space as $\bar{\mathbf{0}}^K = [\sqrt{K}, 0, \dots, 0]^\top$.

Distance The shortest path between two points on the manifold follows the curvature of space and is known as a geodesic. For any two points $\mathbf{x}, \mathbf{y} \in \mathbb{L}_K^n$, the length of the geodesic between them is defined as

$$d_{\mathbb{L}}(\mathbf{x}, \mathbf{y}) = \sqrt{K} \operatorname{acosh} \left(\frac{-\langle \mathbf{x}, \mathbf{y} \rangle_{\mathcal{L}}}{K} \right).$$

The formulation for the squared distance, as proposed by Law et al. (2019), is simpler and can be calculated as

$$d_{\mathbb{L}}^2(\mathbf{x}, \mathbf{y}) = \|\mathbf{x} - \mathbf{y}\|_{\mathbb{L}}^2 = -2K - 2\langle \mathbf{x}, \mathbf{y} \rangle_{\mathcal{L}}.$$

Exponential and Logarithmic Maps. As a Riemannian manifold, the Lorentz space is locally Euclidean, allowing approximation at any point \mathbf{x} using the tangent space $\mathcal{T}_{\mathbf{x}}\mathcal{L}$. We present the exponential and logarithmic maps that move points from and to the tangent space in A.1, along with additional Lorentzian operations.

4. Methodology

4.1. Problem Setting

We are given a set of subject-specific EEG sequences and their corresponding classification labels. Assuming that the set of possible classes is fixed, the objective is to classify new EEG recordings from the same subject based on patterns in the signals. Let $x^{\text{eeg}} \in X^{\text{eeg}} := \mathbb{R}^{C \times T}$ denote an EEG recording with C channels and T time points, $x^{\text{id}} \in X^{\text{id}} := \{1, \dots, S\}$ the subject identifier, and $y \in Y := \{1, \dots, K\}$ the corresponding class label.

Given N samples $\{(x_i^{\text{eeg}}, x_i^{\text{id}}, y_i)\}_{i=1}^N$ drawn from an unknown distribution d , the task is to learn a model that maps unseen EEG recordings x^{eeg} from the same distribution to their ground-truth class y .

4.2. Cross-Subject Training with LoRA

Conventional EEG classification methods typically train separate models for each subject, motivated by the assumption that inter-subject variability in neural patterns and data distributions hinders effective joint training. However, this subject-specific approach suffers from poor generalization: models specialized on individual subjects fail to perform reliably on unseen subjects. In real-world clinical settings, diagnostic predictions are typically made once per subject, and so we do not have labeled instances to train subject-specific models on. This motivates the development of models that generalize well across individuals.

Previous work in this direction embeds the subject information and concatenates it with the channel dimension of the input data to the model, making the subject information available to the model (Burchert et al., 2024). However, this has several disadvantages, especially in convolutional networks, due to the position of the encoding and the lack of control on how it is incorporated with the EEG channel information. To remedy this, we directly incorporate subject ID embeddings in the data transformations by adding subject-specific low-rank adapters (Hu et al., 2022). This allows us to model a richer embedding of the subject information while preserving cross-subject EEG patterns. Let

$$\hat{y} : X^{\text{eeg}} \times X^{\text{id}} \rightarrow Y$$

be an EEG classification model, parametrized by P many parameter matrices $W_p \in \mathbb{R}^{I_p \times J_p}$ ($p = 1:P$). Here, we add low-rank adapter modules to the parameter matrices W_p , replacing the original W_p , now called W_p^{shared} , by a combination of shared and subject-specific parameters:

$$W_p := W_p^{\text{shared}} + Q_p^s (R_p^s)^T, \quad W_p^{\text{shared}} \in \mathbb{R}^{I_p \times J_p}, \quad Q_p^s \in \mathbb{R}^{I_p \times K_p}, \quad R_p^s \in \mathbb{R}^{J_p \times K_p} \quad (1)$$

with a lower rank $K_p \ll I_p, J_p$ for all p .

The model is learned as before, and the total parameter count grows from $\sum_p I_p J_p$ to $\sum_p I_p J_p + (I_p + J_p) K_p S$.

We initialize Q_p^s with a random Gaussian and R_p^s with zeros. Thus, $Q_p^s R_p^{sT}$ is zero at the beginning of training. This enables a rich and lightweight integration of the subject information in the training process because the parameters of the model p are directly dependent on the subject s .

4.3. Lorentz Boost LoRA Layer

We also aim to use the subject-specific LoRAs at the decoder level, however, additive Euclidean updates do not respect the manifold geometry and require subsequent projection operations that may distort the adapted features. To address this, we introduce the Lorentz Boost LoRA (LB-LoRA) layer, which adapts representations using the Lorentz Boost as a native isometry of the hyperbolic space.

Let $\mathbf{x} \in \mathbb{L}_K^n$, be a point on the Lorentz model. A pure Lorentz boost in the unit direction v with rapidity ξ transforms $\mathbf{x} = (x_t, \mathbf{x}_s)$ as:

$$\text{Boost}(h; v, \xi) = \begin{bmatrix} x_t \cosh \xi + (\mathbf{x}_s \cdot v) \sinh \xi \\ \mathbf{x}_s + v [(\mathbf{x}_s \cdot v)(\cosh \xi - 1) + x_t \sinh \xi] \end{bmatrix} \quad (2)$$

For each subject s , we define learnable parameters for r boosts: directions $\{v_i^{(s)}\}_{i=1}^r$ and scalar magnitudes $\{\mu_i^{(s)}\}_{i=1}^r$. The final adapted output $y^{(s)}$ is obtained by sequentially applying these boosts to the shared output:

$$y^{(s)} = \xi^{(s)} \circ \xi_{r-1}^{(s)} \circ \dots \circ \xi_1^{(s)}(h_{shared}) \quad (3)$$

where $\xi_i^{(s)}(h) = \text{Boost}(h; \frac{v_i^{(s)}}{\|v_i^{(s)}\|}, \alpha \cdot \mu_i^{(s)})$ and α is a scaling hyperparameter. This formulation ensures that all adaptations remain on the manifold without requiring artificial projection steps, providing a geometrically consistent method for subject-specific tuning.

4.4. LAtte Model Overview

LAtte is a fully hyperbolic architecture for cross-subject EEG classification that aims to separate and model subject-invariant EEG patterns and subject-specific variability. The model consists of three main stages: a subject-aware EEG processor, a hyperbolic temporal encoder, and a prototype hyperbolic decoder, as shown in Algorithm 1 and Figure 1.

First, raw EEG signals are processed by Euclidean spatial and spatio-temporal convolutional blocks. Here, subject information is injected via LoRAs. This explicitly informs shifts in distributions between subjects. The resulting embeddings are then projected onto the Lorentz manifold, after which all subsequent operations are performed fully in hyperbolic space.

Second, LAtte applies a dual-branch hyperbolic encoder

Algorithm 1 LAtte: Lorentz Attention for EEG Classification

Require: $\mathcal{D}^{\text{train}} = \{(x_n^{\text{eeg}}, x_n^{\text{id}}, y_1), \dots, (x_N^{\text{eeg}}, x_N^{\text{id}}, y_N)\}$, \mathcal{L}^n , $W_{\text{proc}}^{\text{pretrained}}$, $W_{\text{inc}}^{\text{pretrained}}$, number of epochs M
Initialization: $W_{\text{proc}}^{\text{shared}} \leftarrow W_{\text{proc}}^{\text{pretrained}}$
 $W_{\text{IncMax}} \leftarrow W_{\text{inc}}^{\text{pretrained}}$
 $W_{\text{att}}, W_{\text{dec}}^{\text{shared}}, W_{\text{out}}, Q_{\text{dec}} \sim \mathcal{U}(-\sigma, \sigma)$
 $Q_{\text{proc}} \sim \mathcal{N}(\mu, \sigma)$
 $R_{\text{proc}}, R_{\text{dec}} = 0$
for epoch $m = 1$ to M **do**
for each training example $(x_n^{\text{eeg}}, x_n^{\text{id}}, y_n) \in \mathcal{D}^{\text{train}}$ **do**
 $z_n \leftarrow \text{Processor}(x_n^{\text{eeg}}, x_n^{\text{id}}, W_{\text{proc}}^{\text{shared}}; Q_{\text{proc}}, R_{\text{proc}})$ {Eq.13}
 $z_n \leftarrow \text{HyperbolicProjection}(z_n; \mathcal{L}^n)$ {Eq.13}
 $z_n \leftarrow \text{Patching}(z_n)$ {Eq.4}
 $z_{\text{base}} \leftarrow \text{HyperBaselineBlock}(z_n; W_{\text{IncMax}})$ {Eq.12}
 $z_{\text{inc}} \leftarrow \text{HyperInceptionBlock}(z_n)$ {Eq.12}
 $z_n \leftarrow z_{\text{base}} - z_{\text{inc}}$
 $z_n \leftarrow \text{LorentzAttention}(z_n; W_{\text{att}})$ {Eq.17}
 $z_n \leftarrow \text{CentroidUnpatch}(z_n)$ {Eq.14}
 $z_n \leftarrow \text{LorentzFC}(z_n, x_n^{\text{id}}, W_{\text{dec}}^{\text{shared}}; Q_{\text{dec}}, R_{\text{dec}})$ {Eq.10}
 $\hat{y}_n \leftarrow \text{LorentzPrototypeDecoder}(z_n; W_{\text{out}})$ {Eq.10}
 $\ell_n \leftarrow \text{Cross-Entropy}(\hat{y}_n, y_n)$ {Eq.15}
end for
 Compute total loss: $\ell \leftarrow \frac{1}{N} \sum_{n=1}^N \ell_n$
 Update parameters: $W, W^{\text{shared}}, Q_p^s, R_n^p$ based on $\nabla_{\theta} \mathcal{L}$
end for
return W, Q, R

inspired by EEG baseline correction. A baseline branch with average pooling learns a smoothed reference representation, while a task branch with max pooling models the task signals. Their difference is assumed to highlight task-relevant deviations. The embeddings are further fed into a Lorentz attention module to capture long-range temporal dependencies.

Lastly, a hyperbolic random projection layer regularizes and reduces dimensionality, and classification is performed using a Lorentzian prototype decoder based on the squared geodesic distances. The full model is pretrained with self-supervised reconstruction and cut-and-fill tasks and subsequently trained jointly across all subjects, with subject-conditional fine-tuning.

4.4.1. PROCESSOR

The LAtte architecture utilizes both the EEG sequences X^{eeg} and the corresponding subject ids X^{id} as input. We generate initial embeddings z_n of this input using an input processor inspired by Wei et al. (2019). The processor is comprised of two sequential stages, Spatial Component Analysis (SCA) and Spatio-Temporal Filtering (STF). Each stage consists of a convolutional layer followed by batch

normalization. The SCA block transforms the data from the channel domain to a component domain using a kernel of size $(F_T, 1)$. This effectively performs a linear combination across channels. The following STF block uses a kernel of size $(1, F_C)$ to convolve along the time dimension, extracting temporal features. To adapt the model to specific subjects, we inject subject information into both blocks by expanding the weight matrix according to Equation (1), such that $W_{\text{proc}} := W_{\text{proc}}^{\text{shared}} + Q_{\text{proc}}^s (R_{\text{proc}}^s)^T$.

After generating z_n , we map the latent representations onto the Lorentz manifold through a direct time element concatenation. To capture local temporal patterns, the sequence is partitioned into minimally overlapping segments (patches). These patches are encoded and then aggregated using a Lorentzian centroid operation, which computes the hyperbolic average of the patch embeddings. This patching strategy enhances representation learning and improves computational efficiency by reducing the effective sequence length.

Patching We split the embedded EEG sequence into windows with minimal overlap. Let

$$z_n = (z_{n,1}, \dots, z_{n,T}) \in \mathbb{R}^{T \times d}$$

denote the processed EEG sequence. For a fixed number of windows w , we define the window length L and stride g as

$$L := \left\lceil \frac{T}{w} \right\rceil, \quad g := \frac{T - L}{\max(w - 1, 1)}.$$

The patching operator slices z_n into w evenly distributed temporal windows:

$$\begin{aligned} \text{Patching}(z_n) &:= (z_n^{(1)}, \dots, z_n^{(w)}), \\ z_n^{(i)} &:= (z_{n,\tau_i+1}, \dots, z_{n,\tau_i+L}) \in \mathbb{R}^{L \times d}, \quad (4) \\ \tau_i &:= \lfloor (i-1)g \rfloor, \quad i = 1, \dots, w. \end{aligned}$$

The patches are then reshaped to a sequence in $\mathbb{R}^{w \times L \times d}$.

4.4.2. ENCODER

The LAtte encoder is inspired by baseline deduction methods commonly used in EEG analysis. Traditionally, these methods leverage paired recordings where a baseline graph is generated from resting state data and a task graph is generated at task time (Maess et al., 2016). Subtracting the baseline from the task graph isolates task-specific neural activity by mitigating individual variability and signal noise. However, many real-world datasets lack explicit resting state recordings, limiting the applicability of this approach.

To address this challenge, we propose a dual-branch architecture that learns an implicit baseline directly from the task data. The first branch, dubbed the baseline block, employs a Hyperbolic Inception Block with average pooling to estimate a smoothed baseline representation. In parallel, the

second branch uses a Hyperbolic Inception Block with max pooling to highlight strong activation signals, which act as the task graph. We compute the deviation between these two representations (see Figure 1 and Algorithm 1) to produce embeddings that better highlight task-relevant information.

Hyperbolic InceptionTime Block To effectively model latent representations across multiple temporal resolutions and extract meaningful features, we utilize the Inception-Time architecture (Ismail Fawaz et al., 2020). Specifically, we translate the original Euclidean architecture to the Lorentz manifold to capture cross-channel and cross-temporal hierarchical relationships.

The block begins with a bottleneck layer to reduce the channel dimensionality, followed by three parallel convolutional branches with different kernel sizes to capture temporal patterns at multiple resolutions. In parallel, a max-pooling branch is included to emphasize prominent local features. We use our formulation of a Lorentzian maxpool defined in the section below. For the baseline block, we replace the max-pooling with average pooling (Bdeir et al., 2024).

We define the composite convolutional operator

$$\phi_k(\cdot; W) := \text{ReLU}(\text{BN}(\text{Conv1D}_k(\cdot; W))),$$

where Conv1D_k denotes a one-dimensional convolution with kernel size k .

Given input embeddings $z_n \in \mathcal{L}_K^n$, the block first applies a bottleneck projection

$$z_n^{(0)} = \phi_1(z_n; W^{(0)}), \quad W^{(0)} \in \mathbb{R}^{C' \times C \times 1}, \quad (5)$$

where $C' < C$ is the bottleneck dimension.

Next, multiple convolutional branches with different kernel sizes are applied in parallel:

$$z_n^{(i)} = \phi_{k_i}(z_n^{(0)}; W^{(i)}), \quad i = 1, 2, 3 \quad (6)$$

with

$$W^{(i)} \in \mathbb{R}^{C'' \times C' \times k_i}, \quad k_i \in \{k_1, k_2, k_3\},$$

where C'' denotes the number of filters per branch. In addition, a pooling branch is defined as

$$z_n^{(4)} = \phi_{\text{pool}}(z_n^{(0)}; W^{(4)}). \quad (7)$$

The outputs of all branches are combined via direct Lorentz concatenation:

$$z_n^{\text{out}} = \text{HCat}(z_n^{(1)}, z_n^{(2)}, z_n^{(3)}, z_n^{(4)}). \quad (8)$$

Hyperbolic MaxPool We introduce a distance based Lorentzian maxpooling operator. Given a 1D window of width k , stride t , padding u , and dilation δ , we first compute a scalar score for each embedding as the geodesic distance to the origin o :

$$s_{b,\ell} = d_{\mathcal{L}}(x_{b,\ell}, o) = \operatorname{arcosh}(-\langle x_{b,\ell}, o \rangle_L), \quad (9)$$

We then perform Euclidean maxpooling on the scalar score sequence $\{s_{b,\ell}\}_{\ell=1}^L$ to obtain pooled scores and their respective indices. These indices are used to gather hyperbolic vectors from the original input. No transformations are applied to the hyperbolic vectors. Intuitively, this performs the pooling operations as a selection based on geodesic radius. For each window, we select the point furthest from the hyperbolic origin, a choice that correlates with the highest semantic difference in hierarchical embeddings.

4.4.3. RANDOM PROJECTION DECODER

Following the encoder, we apply an LB-LoRA layer to reduce dimensionality and prepare the embeddings for classification. During training, the shared weights $W_{\text{LFC}}^{\text{shared}}$ are randomly initialized and frozen to simulate a random projection, borrowing from the Johnson-Lindenstrauss lemma (Blum, 2005), which states that high-dimensional points can be projected into a lower-dimensional space $k = O(\log n/\varepsilon^2)$ while approximately preserving pairwise distances. By fixing $W_{\text{LFC}}^{\text{shared}} \sim \mathcal{U}(-\sigma, \sigma)$, we effectively perform a dimensionality reduction on the manifold that lowers computational ability and acts as a regularizer. To reintroduce adaptability, we augment this frozen layer with a subject-specific LoRA. We initialize the down-projection Q_{LFC} with the same random distribution as $W_{\text{LFC}}^{\text{shared}}$ to capture features, while the up-projection R_{LFC} is initialized to zero to ensure the initial output matches the random projection. With a learnable scaling factor α_s , the final output Z is defined as:

$$Z = W_{\text{LFC}}^{\text{shared}} Z + \alpha_s R_{\text{LFC}} Q_{\text{LFC}}^T Z \quad (10)$$

The final classification is done using a prototype classifier (Chen et al., 2022) with frozen class embeddings.

4.5. Pretraining

Our architecture relies on the model’s ability to learn rich representations of the input data. However, due to the limited amount of data per subject in smaller datasets, models often overfit to subject-specific noise. To extract meaningful patterns from EEG signals, we therefore propose a multi-subject encoder pertaining. The setting is self-supervised, which allows us to train the model without expert labels. We rely on two main surrogate tasks: cut and fill, and reconstruction.

Cut and Fill randomly select an interval of length l uniformly sampled from a range $[l_{\min}, l_{\max}]$ in the input data. We then replace this interval with the mean of the signal and predict the missing values. The cut-fill can be seen in Algorithm 2. The loss for a given cut-mask M is:

$$L_{\text{cf}} = \frac{1}{\|M\|_1} \|M \odot (\hat{x} - x)\|_F^2, \quad (11)$$

Algorithm 2 Apply-Cut-and-Fill

Require: $x \in \mathbb{R}^{B \times 1 \times C \times T}$
Require: $l_{\min}, l_{\max} \in (0, 1]$
Require: $f \in \mathbb{R}^{1 \times 1 \times C \times 1}$
Ensure: $x^{\text{masked}} \in \mathbb{R}^{B \times 1 \times C \times T}$, $M \in \{0, 1\}^{B \times 1 \times C \times T}$,
 spans $\{(s_b, e_b)\}_{b=1}^B$
 1: $x^{\text{masked}} \leftarrow x$; $M \leftarrow \mathbf{0}_{B \times 1 \times C \times T}$
 2: **for** $b = 1$ **to** B **do**
 3: $\ell_b \sim \text{Unif}(\{[l_{\min}T], \dots, [l_{\max}T]\})$
 4: $s_b \sim \text{Unif}(\{0, \dots, T - \ell_b\})$; $e_b \leftarrow s_b + \ell_b$
 5: **for** $c = 1$ **to** C **do**
 6: **for** $t = s_b$ **to** $e_b - 1$ **do**
 7: $x_{b,1,c,t}^{\text{masked}} \leftarrow f_{1,1,c,1}$
 8: $M_{b,1,c,t} \leftarrow 1$
 9: **end for**
 10: **end for**
 11: **end for**
 12:
 13: **return** x^{masked} , M , $\{(s_b, e_b)\}_{b=1}^B$

Reconstruction The reconstruction task is a self-supervised objective, where the EEG data is passed through the encoder to generate a compact latent representation. This embedding is then fed into the decoder, which attempts to reconstruct the original input signal as closely as possible.

At each pre-training step, we stochastically select a surrogate task: with probability r , we perform a reconstruction update (minimizing L_{recon}), and with probability $1 - r$ we perform a cut-and-fill update (minimizing L_{cf}).

4.6. Subject-conditional Fine-tuning

Despite challenges such as subject-specific noise and distributional shifts, learning shared structure across subjects remains a promising strategy for constructing more robust latent representations. Building on prior work of fine-tuning for EEG Classification (Wei et al., 2019) and cross-subject training with subject features (Burchert et al., 2024), we combine both approaches and propose a fine-tuning protocol with subject features. First, we train the cross-subject model with the LoRA embedding of the subject information and then fine-tune on the individual subject, leveraging universal patterns shared across subjects while making the different distributions explicit to the model.

5. Experiments

Experimental Setup We evaluate our approach on three widely studied EEG datasets, each representing a classification paradigm: motor imagery, steady-state visual responses, and error-related brain activity. For the preprocessing, we follow the common steps and use the same train/val/test splitting protocol as (Pan et al., 2022), where for the tasks of SSVEP and ERN, the data is split session-wise, and for MI, instance-wise for each subject. A detailed description can be found in Section A.3.

We compare our LAtte model against well-established EEG Classification baselines, including ShallowConvNet (Schirrmeyer et al., 2017), EEGNet (Lawhern et al., 2018), SCCNet (Wei et al., 2019), EEG-TCNet (Ingolfsson et al., 2020), TCNet-Fusion (Musallam et al., 2021), FBCNet (Mane et al., 2021), MBEEGSE (Altuwajri et al., 2022), InceptionTime (Burchert et al., 2024), MAtt (Pan et al., 2022), CBraMod (Wang et al., 2025), HyperMatt (Bdeir et al., 2025), and TCFormer (Altaheri et al., 2025) across three commonly used datasets. Furthermore, we include three cross-subject baselines: ResNetJoint, MAttJoint, and InceptionJoint (Burchert et al., 2024). For the MI and SSVEP datasets, accuracy is used as the performance metric, while AUC is employed for ERN due to a class imbalance. For LAtte, we first pre-train the model with the reconstruction task and load the resulting weights for the processor and HyperBaselineBlock. In the main training loop, LAtte is trained on all subjects jointly.

Hyperparameters were selected based on validation performance. The search ranges and optimal configurations for each dataset are reported in Section A.4. LAtte is trained for 200 epochs, and test performance is reported at the epoch with the best validation score. Experiments are repeated 10 times with different random seeds.

Performance Comparison In Table 1, we compare our proposed model with current state-of-the-art baselines, where baseline results are aggregated from Pan et al. (2022); Burchert et al. (2024); Bdeir et al. (2025). Additionally, we run TCFormer as the most recent baseline and CBraMod as the representative for the foundation model literature on our selection of tasks and optimize their hyperparameters based on validation performance for each dataset individually.

The first table block reports results in the subject-specific (SS) setting, where a separate model is trained for each subject, and the final performance is averaged across subjects. The second block presents results in the subject-conditional (SC) setting, where a single model is trained across all subjects with additional subject meta-features (e.g., subject ID).

In the SC setting, LAtte achieves a significant performance improvement over all baselines across tasks. Unlike existing models that rely on static subject embeddings, LAtte

Table 1. Performance comparison on the EEG datasets MI, SSVEP, and ERN. We repeated the experiments 10 times on random seeds and report the average accuracy for MI and SSVEP and the AUC for ERN. The best result is highlighted in bold, the second best underlined. The first block contains subject-specific (SS) models, where one model is trained per subject. In the second block are subject-conditional (SC) models, where the model is trained across subjects with additional subject information.

Models	MI	SSVEP	ERN
ShallowConvNet	61.84±6.39	56.93±6.97	71.86±2.64
EEGNet	57.43±6.25	53.72±7.23	74.28±2.47
SCCNet	71.95±5.05	62.11±7.70	70.93±2.31
EEG-TCNet	67.09±4.66	55.45±7.66	77.05±2.46
TCNet-Fusion	56.52±3.07	45.00±6.45	70.46±2.94
FBCNet	71.45±4.45	53.09±5.67	60.47±3.06
MBEEGSE	64.58±6.07	56.45±7.27	75.46±2.34
InceptionTime	62.85±3.21	62.71±2.95	73.55±5.08
MAtt	74.71 ±5.01	65.50±8.20	76.01±2.28
CBraMod	45.22±1.26	40.45±2.12	68.49±1.17
HyperMAtt	74.12±2.91	68.10±2.41	78.01±1.30
TCFormer	71.31±2.22	47.64±3.10	78.82±1.68
LAtte + FT	73.77±3.11	73.75 ±2.05	81.70 ±1.72
ResNetJoint	55.54±2.72	54.15±1.19	73.09±0.72
MAttJoint	61.13±0.56	60.71±0.29	75.78±1.23
InceptionJoint	61.38±1.57	66.00±0.36	76.13±0.95
LAtte	71.63 ±2.80	71.53 ±1.00	81.57 ±1.22
SS: Relative Δ	-1.25%	8.30%	4.73%
SC: Relative Δ	16.67%	8.38%	7.15%

leverages a richer LoRA-based subject representation, enabling better separation of subject-specific noise. In addition, LAtte outperforms the subject-specific baselines on SSVEP and ERN tasks, highlighting the benefits of its more expressive hyperbolic representation.

For the subject-specific (SS) setting, we fine-tune the cross-subject model separately for each subject using only that subject’s data and ID. We report the mean across subjects and the pooled standard deviation over runs, with per-subject results in Section A.4. Fine-tuning enables direct adaptation to each subject’s data distribution while retaining subject-invariant structure learned during joint training, and converges within only a few iterations due to the strong initialization and fully subject-dependent LoRA pre-decoder.

Foundation models such as LaBram (Jiang et al., 2024) and its successor CBraMod (Wang et al., 2025) underperform on these small-scale EEG datasets. In particular, their fixed patch length of 200 is poorly matched to the short sequence lengths of MI (438), SSVEP (128), and ERN (160), leading to extensive zero padding and preventing them from effectively leveraging their main advantage in large-scale pretraining. Additionally, it should be noted that our reproduced TCFormer results on MI are lower than those reported in the original paper. This is because their model was tuned directly on the test set without a validation split. TCFormer remains a strong baseline for MI and ERN. However, it struggles with large inter-subject vari-

Table 2. Component Analysis of LAtte. We compare the performance of the full LAtte model to versions without the main modules on SSVEP. We report the accuracy and std over 5 runs.

Model Variant	Accuracy	Δ
LAtte Full	71.53±1.00	-
LAtte w/o Lorentz	57.40±6.53	-19.75%
LAtte w/o LoRA	62.87±0.51	-12.11%
LAtte w/o Proj	69.34±1.37	-3.06%
LAtte w/o Cut/Fill	69.55±0.71	-2.77%
LAtte w/o Pretrain	69.71±0.68	-2.54%

ability in SSVEP, where 3 of 11 subjects normally achieve near-random performance (Table 5). In contrast, LAtte generalizes consistently across all three tasks, benefiting from richer hyperbolic embeddings and task-specific shared weights across subjects, which improve performance on these challenging subject distributions.

Ablation Studies In Table 2, we analyze the contribution of each component in the LAtte architecture by removing one module at a time. The largest performance drop occurs when replacing the Lorentz manifold with Euclidean space. Here, accuracy decreases by 19.75%, confirming the importance of a more expressive geometric representation. Removing the subject-dependent LoRA parameters also leads to a substantial drop by 12.11%, as the model can no longer effectively distinguish subject-specific distributions, which is critical for cross-subject generalization. The decoder projection and cut/fill augmentation contribute to improved regularization and stable convergence, which is an essential property for small EEG datasets. Finally, pretraining the processor and encoder provides additional gains by offering more stable initialization.

LOSO To evaluate generalization to unseen subjects, we adopt the leave-one-subject-out (LOSO) protocol (Kunjan et al., 2021). Under this scheme, the model is trained on data from all but one subject, with the held-out subject used exclusively for testing. This process is repeated such that each subject serves once as the test subject. The final performance is averaged across all folds. For training and validation, we follow the same splitting strategy described in Section A.3: an instance-wise split for MI, and a session-wise split for SSVEP and ERN.

As baselines, we consider TCFormer (Altaheri et al., 2025), which employs the same protocol for cross-subject evaluation, and CBraMod (Wang et al., 2025), which originally uses a fixed hold-out set of subjects for validation. However, fixed subject splits can lead to biased or unstable estimates due to extreme inter-subject variability. To ensure a fair comparison, we also evaluate CBraMod under the LOSO protocol. All reported results in Table 3 are averaged over

Table 3. Performance comparison for LOSO protocol. We repeated the experiments 5 times on random seeds and report the average accuracy for MI and SSVEP and the AUC for ERN.

Models	MI	SSVEP	ERN
CBraMod	35.26±1.51	43.58±2.63	66.70±2.99
TCFormer	39.84±3.21	42.18±3.91	74.28±4.10
LAtte	42.31±1.46	57.86±3.66	75.31±3.17

five runs with different random seeds.

As expected, all models exhibit a substantial drop in performance under LOSO, reflecting the strong distribution shifts between subjects. This degradation is particularly pronounced for CBraMod and TCFormer on MI and SSVEP, where inter-subject variability is known to be severe. In contrast, LAtte achieves consistently higher performance across tasks. For SSVEP, this suggests that LAtte more effectively isolates task-relevant structure in the shared weights W^{shared} , while relegating subject-specific variability to the LoRA parameters Q, R . These subject parameters are set to zero for unseen subjects during training due to the initialization just leaving the learned shared patterns in W^{shared} . On ERN, both LAtte and TCFormer generalize relatively well across subjects, leading to a similar reduction in performance, though LAtte maintains a consistent advantage. While true cross-subject generalization remains challenging, explicitly conditioning model parameters on the subject appears to be a promising direction.

Runtime Comparison We adopt the parametrization trick in the CUDA implementations of Bdeir et al. (2025), enabling efficient computation of hyperbolic operations. As a result, LAtte is substantially faster, requiring only 0.364s per epoch compared to 1.519s for TCFormer and 4.0s for MAtt, corresponding to speedups of 4.2× and 11×, respectively. All timings were measured on the SSVEP task using an NVIDIA GeForce RTX 4070 Ti. In addition, the subject-specific components are lightweight due to the use of LoRA. Out of the 1.2M parameters in LAtte, 278k are allocated to subject-specific adaptation.

6. Conclusion

In this work, we introduced LAtte, a novel hyperbolic framework for cross-subject EEG classification that unifies Lorentzian attention with an InceptionTime-based encoder. By combining subject-specific low-rank adapters with hyperbolic representations, LAtte effectively learns shared neural patterns from subject-dependent variability. This design enables a single unified model to generalize across individuals while maintaining adaptability to new, unseen subjects. The proposed cross-subject LAtte outperforms most of its subject-specific counterparts. Our results on three well-established datasets prove that hyperbolic geom-

etry offers a natural and strong inductive bias for modeling the hierarchical structure inherent in EEG data, and subject-adaptive mechanisms such as LoRA can enable scalable, generalizable EEG decoding. LAtte attempts to build on previous approaches to reduce classification sensitivity to noise and, become more accessible in real-world clinical applications.

7. Impact Statement

Ethics We are committed to contributing positively to society and human well-being, while respecting the privacy of the subjects involved in our evaluation. Our experiments utilize three established EEG datasets: MI, SSVEP, and ERN, which involve data from human subjects. These datasets are fully anonymized and do not contain any personally identifiable information. Additionally, they are publicly available and widely used within the machine learning community.

Reproducibility We are committed to ensuring the reproducibility of our model, LAtte. To support this, we provide the source code, including pre-processing steps, model architecture, and training scripts, in the supplementary material. Upon publication, the code will also be made publicly available on GitHub, along with detailed documentation to guide experiment setup and execution. Additionally, we commit to releasing the pretrained checkpoints used for writing this paper. The datasets used in our experiments are publicly available, and we additionally provide a link to the preprocessed data in a cloud service for easy access. All hyperparameters and model configurations are detailed in both the paper and the code repository to ensure easy replication.

References

- Altaheri, H., Karray, F., and Karimi, A.-H. Temporal convolutional transformer for eeg based motor imagery decoding. *Scientific Reports. Nature*, 15(1):32959, 2025.
- Altuwaijri, G. A., Muhammad, G., Altaheri, H., and Al-sulaiman, M. A multi-branch convolutional neural network with squeeze-and-excitation attention blocks for eeg-based motor imagery signals classification. *Diagnostics*, 12(4):995, 2022.
- Atigh, M. G., Schoep, J., Acar, E., van Noord, N., and Mettes, P. Hyperbolic image segmentation. In *Proceedings of the IEEE/CVF Conference on Computer Vision and Pattern Recognition (CVPR)*, pp. 4453–4462, June 2022.
- Bdeir, A., Schwethelm, K., and Landwehr, N. Fully hyperbolic convolutional neural networks for computer vision. In *The Twelfth International Conference on Learning Representations, ICLR 2024, Vienna, Austria, May 7-11, 2024*. OpenReview.net, 2024. URL <https://openreview.net/forum?id=ekz1hN5QNh>.
- Bdeir, A., Burchert, J., Schmidt-Thieme, L., and Landwehr, N. Robust hyperbolic learning with curvature-aware optimization. *Neurips 2025*, 2025.
- Blum, A. Random projection, margins, kernels, and feature-selection. In *Proceedings of the 2005 International Conference on Subspace, Latent Structure and Feature Selection, SLSFS’05*, pp. 52–68, Berlin, Heidelberg, 2005. Springer-Verlag. ISBN 3540341374. doi: 10.1007/11752790_3. URL https://doi.org/10.1007/11752790_3.
- Brunner, C., Leeb, R., Müller-Putz, G., Schlögl, A., and Pfurtscheller, G. Bci competition 2008–graz data set a. *Institute for Knowledge Discovery (Laboratory of Brain-Computer Interfaces), Graz University of Technology*, 16: 1–6, 2008.
- Burchert, J., Werner, T., Yalavarthi, V. K., de Portugal, D. C., Stubbemann, M., and Schmidt-Thieme, L. Are eeg sequences time series? eeg classification with time series models and joint subject training. *arXiv preprint arXiv:2404.06966*, 2024.
- Chen, W., Han, X., Lin, Y., Zhao, H., Liu, Z., Li, P., Sun, M., and Zhou, J. Fully hyperbolic neural networks. In Muresan, S., Nakov, P., and Villavicencio, A. (eds.), *Proceedings of the 60th Annual Meeting of the Association for Computational Linguistics (Volume 1: Long Papers), ACL 2022, Dublin, Ireland, May 22-27, 2022*, pp. 5672–5686. Association for Computational Linguistics, 2022. doi: 10.18653/v1/2022.ACL-LONG.389. URL <https://doi.org/10.18653/v1/2022.acl-long.389>.
- Cimtay, Y. and Ekmekcioglu, E. Investigating the use of pretrained convolutional neural network on cross-subject and cross-dataset EEG emotion recognition. *Sensors*, 20(7):2034, 2020. doi: 10.3390/S20072034. URL <https://doi.org/10.3390/s20072034>.
- Croft, R. J. and Barry, R. J. Removal of ocular artifact from the eeg: a review. *Neurophysiologie Clinique/Clinical Neurophysiology*, 30(1):5–19, 2000.
- Delorme, A. Eeg is better left alone. *Scientific Reports*, 13(1):2372, 2023.
- Ganea, O.-E., Bécigneul, G., and Hofmann, T. Hyperbolic neural networks, 2018. URL <https://arxiv.org/abs/1805.09112>.
- Hu, E. J., Shen, Y., Wallis, P., Allen-Zhu, Z., Li, Y., Wang, S., Wang, L., and Chen, W. Lora: Low-rank adaptation of large language models. In *The Tenth International Conference on Learning Representations, ICLR*

- 2022, *Virtual Event, April 25-29, 2022*. OpenReview.net, 2022. URL <https://openreview.net/forum?id=nZeVKeeFYf9>.
- Ingolfsson, T. M., Hersche, M., Wang, X., Kobayashi, N., Cavigelli, L., and Benini, L. Eeg-tnet: An accurate temporal convolutional network for embedded motor-imagery brain-machine interfaces. In *2020 IEEE Int. Conf. on SMC*, pp. 2958–2965, 2020.
- Ismail Fawaz, H., Lucas, B., Forestier, G., Pelletier, C., Schmidt, D. F., Weber, J., Webb, G. I., Idoumghar, L., Muller, P.-A., and Petitjean, F. Inceptiontime: Finding alexnet for time series classification. *Data Mining and Knowledge Discovery*, 34(6):1936–1962, 2020.
- Jiang, W., Zhao, L., and Lu, B. Large brain model for learning generic representations with tremendous EEG data in BCI. In *The Twelfth International Conference on Learning Representations, ICLR 2024, Vienna, Austria, May 7-11, 2024*. OpenReview.net, 2024. URL <https://openreview.net/forum?id=QzTpTRVtrP>.
- Johnson, W. B., Lindenstrauss, J., et al. Extensions of lipschitz mappings into a hilbert space. *Contemporary mathematics*, 26(189-206):1, 1984.
- Kim, S., Jeong, B., and Kwak, S. HIER: metric learning beyond class labels via hierarchical regularization. In *IEEE/CVF Conference on Computer Vision and Pattern Recognition, CVPR 2023, Vancouver, BC, Canada, June 17-24, 2023*, pp. 19903–19912. IEEE, 2023. doi: 10.1109/CVPR52729.2023.01906. URL <https://doi.org/10.1109/CVPR52729.2023.01906>.
- Kotte, S. and Dabbakuti, J. K. Methods for removal of artifacts from eeg signal: A review. In *Journal of Physics: Conference Series*, volume 1706, pp. 012093. IOP Publishing, 2020.
- Kunjan, S., Grummett, T. S., Pope, K. J., Powers, D. M., Fitzgibbon, S. P., Bastiampillai, T., Battersby, M., and Lewis, T. W. The necessity of leave one subject out (loso) cross validation for eeg disease diagnosis. In *International conference on brain informatics*, pp. 558–567. Springer, 2021.
- Law, M., Liao, R., Snell, J., and Zemel, R. Lorentzian distance learning for hyperbolic representations. In *International Conference on Machine Learning*, pp. 3672–3681. PMLR, 2019.
- Lawhern, V. J., Solon, A. J., Waytowich, N. R., Gordon, S. M., Hung, C. P., and Lance, B. J. Eegnet: a compact convolutional neural network for eeg-based brain-computer interfaces. *Journal of Neural Engineering*, 15(5), 2018.
- Li, J., Qiu, S., Shen, Y., Liu, C., and He, H. Multi-source transfer learning for cross-subject EEG emotion recognition. *IEEE Trans. Cybern.*, 50(7):3281–3293, 2020. doi: 10.1109/TCYB.2019.2904052. URL <https://doi.org/10.1109/TCYB.2019.2904052>.
- Li, X., Song, D., Zhang, P., Zhang, Y., Hou, Y., and Hu, B. Exploring eeg features in cross-subject emotion recognition. *Frontiers in neuroscience*, 12:162, 2018.
- Lotte, F., Congedo, M., Lécuyer, A., Lamarche, F., and Arnaldi, B. A review of classification algorithms for eeg-based brain-computer interfaces. *Journal of Neural Engineering*, 4(2):R1, 2007.
- Maess, B., Schröger, E., and Widmann, A. High-pass filters and baseline correction in m/eeg analysis. commentary on: “how inappropriate high-pass filters can produce artefacts and incorrect conclusions in erp studies of language and cognition”. *Journal of Neuroscience Methods*, 266:164–165, 2016. ISSN 0165-0270. doi: <https://doi.org/10.1016/j.jneumeth.2015.12.003>. URL <https://www.sciencedirect.com/science/article/pii/S0165027015004434>.
- Mane, R., Chew, E., Chua, K., Ang, K. K., Robinson, N., Vinod, A. P., Lee, S.-W., and Guan, C. Fbcnet: A multi-view convolutional neural network for brain-computer interface. *arXiv preprint arXiv:2104.01233*, 2021.
- Margaux, P., Emmanuel, M., Sébastien, D., Olivier, B., and Jérémie, M. Objective and subjective evaluation of online error correction during p300-based spelling. *Advances in Human-Computer Interaction*, 2012:4–4, 2012.
- Mettes, P., Atigh, M. G., Keller-Ressel, M., Gu, J., and Yeung, S. Hyperbolic deep learning in computer vision: A survey. *Int. J. Comput. Vis.*, 132(9):3484–3508, 2024. doi: 10.1007/S11263-024-02043-5. URL <https://doi.org/10.1007/s11263-024-02043-5>.
- Musallam, Y. K., AlFassam, N. I., Muhammad, G., Amin, S. U., Alsulaiman, M., Abdul, W., Altaheri, H., Bencherif, M. A., and Algabri, M. Electroencephalography-based motor imagery classification using temporal convolutional network fusion. *Biomedical Signal Processing and Control*, 69:102826, 2021.
- Muthukumaraswamy, S. D. High-frequency brain activity and muscle artifacts in meg/eeg: a review and recommendations. *Frontiers in Human Neuroscience*, 7:138, 2013.
- Nagano, Y., Yamaguchi, S., Fujita, Y., and Koyama, M. A wrapped normal distribution on hyperbolic space for gradient-based learning. In *International conference on machine learning*, pp. 4693–4702. PMLR, 2019.

- Nguyen, X. S., Yang, S., and Histace, A. Neural networks on symmetric spaces of noncompact type. In *The Thirteenth International Conference on Learning Representations*, 2025.
- Nikolopoulos, S. Mamem eeg ssvep dataset ii (256 channels, 11 subjects, 5 frequencies presented simultaneously). 2021.
- Obeid, I. and Picone, J. The temple university hospital eeg data corpus. *Frontiers in neuroscience*, 10:196, 2016.
- Pan, Y.-T., Chou, J.-L., and Wei, C.-S. Matt: A manifold attention network for eeg decoding. *Advances in Neural Information Processing Systems*, 35:31116–31129, 2022.
- Parbat, D. and Chakraborty, M. A novel methodology to study the cognitive load induced eeg complexity changes: Chaos, fractal and entropy based approach. *Biomedical Signal Processing and Control*, 64:102277, 2021.
- Pion-Tonachini, L., Kreutz-Delgado, K., and Makeig, S. Iclabel: An automated electroencephalographic independent component classifier, dataset, and website. *NeuroImage*, 198:181–197, 2019.
- Roy, Y., Banville, H., Albuquerque, I., Gramfort, A., Falk, T. H., and Faubert, J. Deep learning-based electroencephalography analysis: a systematic review. *Journal of Neural Engineering*, 16(5):051001, 2019.
- Schirrneister, R. T., Springenberg, J. T., Fiederer, L. D. J., Glasstetter, M., Eggenberger, K., Tangermann, M., Hutter, F., Burgard, W., and Ball, T. Deep learning with convolutional neural networks for eeg decoding and visualization. *Human Brain Mapping*, 38(11):5391–5420, 2017.
- Shen, X., Liu, X., Hu, X., Zhang, D., and Song, S. Contrastive learning of subject-invariant EEG representations for cross-subject emotion recognition. *IEEE Trans. Affect. Comput.*, 14(3):2496–2511, 2023. doi: 10.1109/TAFFC.2022.3164516. URL <https://doi.org/10.1109/TAFFC.2022.3164516>.
- Wang, J., Zhao, S., Luo, Z., Zhou, Y., Jiang, H., Li, S., Li, T., and Pan, G. Cbramod: A criss-cross brain foundation model for EEG decoding. In *The Thirteenth International Conference on Learning Representations, ICLR 2025, Singapore, April 24-28, 2025*. OpenReview.net, 2025. URL <https://openreview.net/forum?id=NPNUHgHF2w>.
- Wang, Y., Liu, J., Ruan, Q., Wang, S., and Wang, C. Cross-subject eeg emotion classification based on few-label adversarial domain adaption. *Expert Systems with Applications*, 185:115581, 2021.
- Wei, C.-S., Koike-Akino, T., and Wang, Y. Spatial component-wise convolutional network (sccnet) for motor-imagery eeg classification. In *2019 9th International IEEE/EMBS Conference on Neural Engineering (NER)*, pp. 328–331, 2019.

A. Appendix

A.1. Additional Hyperbolic Operations

Lorentz Concatenation Let $z_n^{(i)} = (z_{n,t}^{(i)}, z_{n,v}^{(i)}) \in \mathcal{L}_K^{d_i}$, where $z_{n,t}^{(i)}$ and $z_{n,v}^{(i)}$ denote the time and space components, respectively. We define

$$\text{HCat}(z_n^{(1)}, \dots, z_n^{(N)}) = \left(\sqrt{\sum_{i=1}^N \|z_{n,v}^{(i)}\|^2 + \frac{N-1}{K}}, z_{n,v}^{(1)}, \dots, z_{n,v}^{(N)} \right). \quad (12)$$

Exp and Log Maps The exponential map $\mathcal{T}_x \rightarrow \mathbb{L}_K^n$ projects tangent vectors onto the manifold via:

$$\exp_x^K(\mathbf{z}) = \cosh(\alpha)\mathbf{x} + \sinh(\alpha)\frac{\mathbf{z}}{\alpha}, \quad \alpha = \sqrt{1/K} \|\mathbf{z}\|_{\mathbb{L}}, \quad (13)$$

where $\|\mathbf{z}\|_{\mathbb{L}} = \sqrt{\langle \mathbf{z}, \mathbf{z} \rangle_{\mathcal{L}}}$. The inverse operation, the logarithmic map, is given by:

$$\log_x^K(\mathbf{y}) = \frac{\text{acosh}(\beta)}{\sqrt{\beta^2 - 1}}(\mathbf{y} - \beta\mathbf{x}), \quad \beta = -\frac{1}{K} \langle \mathbf{x}, \mathbf{y} \rangle_{\mathcal{L}}.$$

Lorentzian Centroid (Law et al., 2019) derive a closed-form for a Lorentzian centroid $\mu_{\mathbb{L}}$ based on the square distances. For points $\{\mathbf{x}_i\}_{i=1}^m \subset \mathbb{L}_K^n$ with weights $\nu \in \mathbb{R}^m$, it is computed as:

$$\mu_{\mathbb{L}} = \frac{\sqrt{K} \cdot \sum_{i=1}^m \nu_i \mathbf{x}_i}{\left\| \sum_{i=1}^m \nu_i \mathbf{x}_i \right\|_{\mathcal{L}}}, \quad (14)$$

where $\|\mathbf{z}\|_{\mathcal{L}} := \sqrt{|\langle \mathbf{z}, \mathbf{z} \rangle_{\mathcal{L}}|}$ ensures normalization to the hyperboloid surface. This closed-form solution approximates the centroid while maintaining manifold constraints.

Lorentz Prototype Decoder A strength of hyperbolic machine learning approaches is the ability to produce fine embeddings for input data while minimally distorting the hierarchical relationships between them. This leads to a better use of the ambient embedding space and better instance clustering. To leverage this, we utilize prototypical classification heads. As opposed to the MLR classifier proposed in (Bdeir et al., 2024), prototype classifiers employ class embeddings as cluster points and outputs the results as distances to each cluster midpoint. The center with minimal distance is the the most similar semantically and is used as the classified class. The Lorentzian prototype decoder in this work is the direct translation of the decoder proposed by (Wang et al., 2021). We first randomly initialize N points on the hyperboloid using the Wrapped Normal Lorentz distribution in (Nagano et al., 2019). We then measure similarity using the square distance as it is better defined and computationally more efficient.

Additionally, this layer can be set to non-learnable, which forces the class centroids to remain static during the training process. This leads to better generalization in some datasets and avoids overfitting. We use cross-entropy as the objective function. Thus,

$$\ell(X^{\text{eeg}}, X^{\text{id}}, y; W; \mathcal{L}) := \frac{1}{N} \sum_{n=1}^N \text{cross-entropy}(y_n, \hat{y}_n) \quad \text{with } \hat{y} := \text{LAtte}(X^{\text{eeg}}, X^{\text{id}}; W; \mathcal{L}) \quad (15)$$

A.2. LAtte

In Figure 1, we show the LAtte architecture overview. It is composed of several modular components that together form a unified, fully hyperbolic learning pipeline. A subject-aware EEG processor extracts low-level spatio-temporal features while injecting subject identity through low-rank adapters. These features are mapped to the Lorentz manifold and passed to a dual-branch hyperbolic encoder, which separates smooth baseline structure from salient task-related activity using

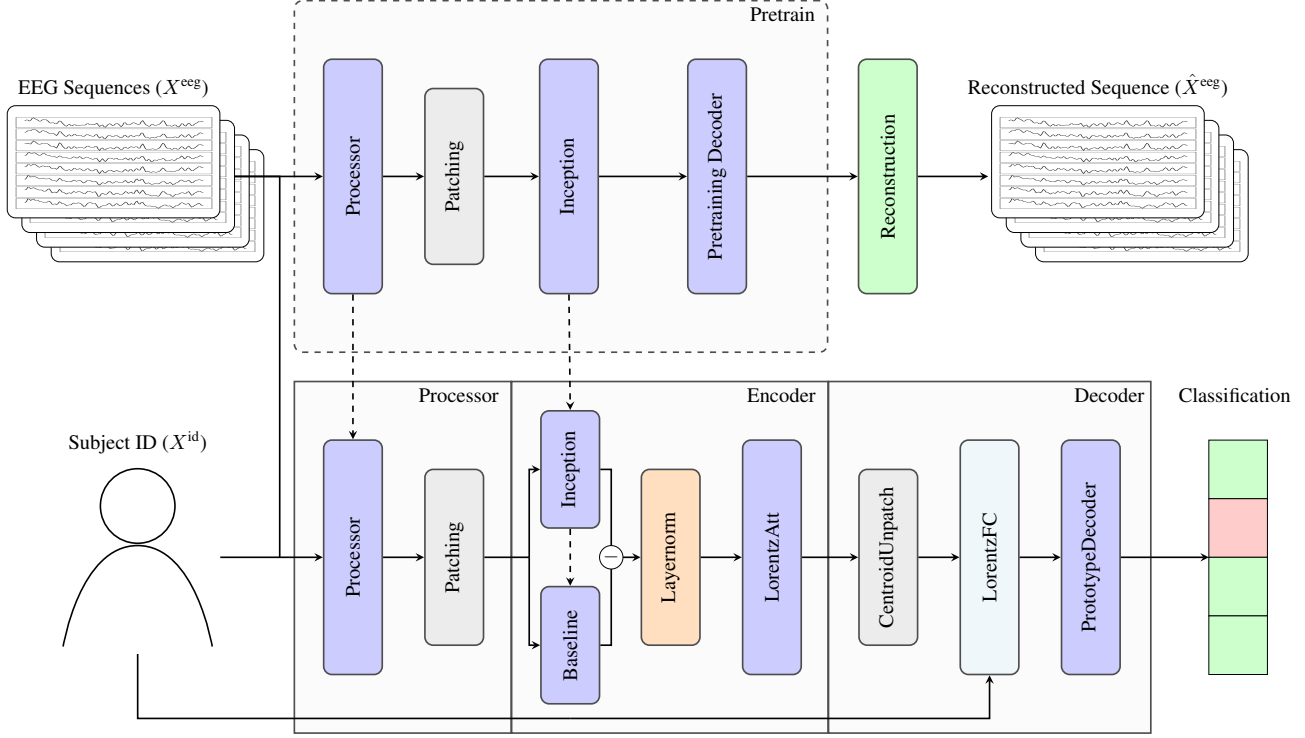


Figure 1. LAtte architecture overview.

complementary pooling strategies. The resulting representations are refined by a Lorentz attention module to capture long-range temporal dependencies. Subject-specific Lorentz Boost LoRA layers then adapt embeddings directly in hyperbolic space, enabling personalized modeling without violating manifold constraints. Finally, a hyperbolic random projection layer regularizes the representation, and a Lorentzian prototype decoder performs classification based on geodesic similarity. The pertaining decoder is depicted in Figure 2

Lorentz Fully Connected Layer After the Lorentz Attention, we apply an LFC to reduce the dimensionality and prepare the embedding for the final classification output. During the training, the $W_{\text{LorentzFC}}^{\text{shared}}$ are frozen to simulate a random projection following the Johnson-Lindenstrauss lemma (Johnson et al., 1984), which states that a set of points in a high-dimensional space can be embedded into a space of much lower dimension in such a way that distances between points are preserved. Let $0 < \varepsilon < 1$ and $X \subset \mathbb{R}^d$ be a set of n points. There exists a linear map:

$$f : \mathbb{R}^d \rightarrow \mathbb{R}^k, \quad k = O\left(\frac{\log n}{\varepsilon^2}\right),$$

By freezing the LFC with randomly initialized weights $W_{\text{LFC}}^{\text{shared}} \sim \mathcal{U}(-\sigma, \sigma)$, we are projecting the embeddings on the manifold to a lower dimension, reducing computational cost and adding regularization. To compensate for the frozen weights, we add a LoRA again to learn subject-specific features and improve the encoding for the final classification, where Q_{LFC} follows the same initialization as $W_{\text{LFC}}^{\text{shared}}$ and R_{LFC} is set to zero. In addition, we set a learning rate α_s . Thus, the output is defined as:

$$Z = W_{\text{LFC}}^{\text{shared}} Z + \alpha_s Q_{\text{LFC}} R_{\text{LFC}}^T Z \quad (16)$$

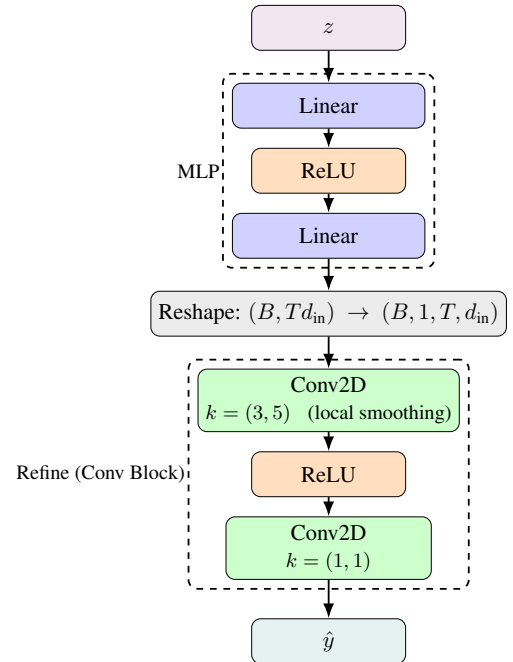


Figure 2. Euclidean decoder used in the reconstruction and cutoff pretraining

Table 4. Overview of the datasets used for the LAtte evaluation.

Dataset	Subjects	Instances	Channels	Timesteps	Classes	Task
BCIC IV-2a	9	7452	22	438	4	Motor Imagery
MAMEM II	11	5500	8	128	5	Visual Stimulus
BCI Challenge	16	5440	56	160	2	Error recognition

Lorentz Multi-Head Attention We compute Lorentzian queries, keys, and values with Lorentz Fully Connected layers (LFC) on the manifold:

$$Q = \text{LFC}_q(X), \quad K = \text{LFC}_k(X), \quad V = \text{LFC}_v(X).$$

The attention weights are obtained from scaled Lorentzian squared distances

$$\alpha_{ij} = \frac{\exp\left(-\frac{\lambda}{\tau} d_{\mathcal{L}}^2(Q_i, K_j)\right)}{\sum_{j'} \exp\left(-\frac{\lambda}{\tau} d_{\mathcal{L}}^2(Q_i, K_{j'})\right)},$$

where λ is a learnable scaling factor and τ is the temperature. Values are aggregated by the Lorentzian weighted centroid

$$\tilde{V}_i = \text{Centroid}_{\mathcal{L}}(V_j, \alpha_{ij}),$$

and the final output is given by

$$\text{LorentzAtt}(X) = \text{LFC}_o(\tilde{V}), \tag{17}$$

with LFC_o a Lorentz fully connected layer.

A.3. Datasets

MI — Motor Imagery (Brunner et al., 2008). The MI dataset, originally released as BCI Competition IV-2a (2008), is a cornerstone benchmark for motor imagery classification. It contains EEG recordings from 9 subjects, acquired with 22 Ag/AgCl electrodes over central and surrounding scalp regions at a sampling rate of 250 Hz. The experimental task involves four motor imagery conditions: right hand, left hand, feet, and tongue. Following established preprocessing protocols, signals were down-sampled to 128 Hz, band-pass filtered to 4–38 Hz, and segmented into 4-second epochs starting 0.5 s post-cue, yielding 438 time points per trial across 22 channels.

SSVEP — Steady-State Visual Evoked Potentials (Nikolopoulos, 2021). The SSVEP dataset (MAMEM II, 2016) targets frequency-tagged visual responses. EEG was collected from 11 subjects using the EGI 300 Geodesic EEG System. Participants fixated on one of five flickering visual stimuli (6.66, 7.50, 8.57, 10.00, 12.00 Hz) for 5-second intervals. Preprocessing retained 1–50 Hz activity and focused on 8 occipital channels (PO7, PO3, POz, PO4, PO8, O1, Oz, O2), corresponding to the visual cortex. Each trial was partitioned into four non-overlapping 1-second segments (125 samples per channel), producing 500 trials per subject of 8-channel SSVEP data.

ERN — Error-Related Negativity (Margaux et al., 2012). The ERN dataset, released as part of the 2015 BCI Challenge¹, captures error-related brain responses during a P300-based spelling task. EEG was recorded from 16 subjects using 56 Ag/AgCl electrodes at 600 Hz. The task poses a binary classification problem, with a natural imbalance favoring correct responses. Preprocessing included down-sampling to 128 Hz and band-pass filtering between 1–40 Hz. Each trial was represented by 56 channels with 160 time points, offering a challenging benchmark due to its class imbalance and inter-subject variability.

Data splitting To reflect realistic BCI usage, we adopt a subject-specific training scheme proposed by (Pan et al., 2022) in which data is split within each subject. For BCIC-IV-2a, the first session is used for training, with one out of eight trials reserved for validation, and evaluation is performed on the second session. For MAMEM-SSVEP-II and BCI-ERN, the first four sessions are used for training, with one out of four trials held out for validation, and testing is conducted on the remaining sessions.

¹<https://www.kaggle.com/c/inria-bci-challenge>

Table 5. Performance Comparison on the SSVEP dataset for the subject-specific case. We report the average accuracy over 10 runs, respectively.

Subject	InceptionTime	MAtt	HyperMAtt	LAte
1	80.40 ± 2.06	81.60 ± 2.87	<u>89.94</u> ± 1.29	90.00 ± 2.18
2	86.60 ± 1.62	89.40 ± 1.36	<u>90.31</u> ± 0.96	94.50 ± 4.62
3	61.60 ± 3.07	58.20 ± 5.64	<u>68.05</u> ± 3.06	74.20 ± 0.16
4	25.00 ± 4.00	20.60 ± 3.88	<u>30.00</u> ± 0.58	42.67 ± 1.89
5	25.00 ± 6.72	26.40 ± 4.80	<u>30.96</u> ± 1.53	53.20 ± 2.34
6	79.20 ± 1.72	79.00 ± 2.68	<u>80.90</u> ± 1.55	86.40 ± 0.70
7	69.20 ± 1.72	66.00 ± 2.19	<u>69.08</u> ± 2.08	78.60 ± 2.07
8	23.60 ± 1.74	23.80 ± 2.71	29.04 ± 0.58	<u>25.20</u> ± 2.03
9	79.40 ± 2.58	88.20 ± 2.04	93.02 ± 3.61	<u>91.80</u> ± 2.84
10	68.60 ± 3.72	70.60 ± 4.54	<u>75.11</u> ± 2.00	76.80 ± 1.38
11	91.20 ± 2.48	90.20 ± 1.47	<u>92.96</u> ± 1.15	94.80 ± 2.57
Summary	62.71±2.95	63.90±1.95	68.12±1.91	73.47±1.82

Table 6. Optimal hyperparameter settings.

Hyperparameter	BCI	SSVEP	ERN
Batch Size	32	32	32
Learning Rate	$1e^{-3}$	$1e^{-3}$	$1e^{-4}$
Weight Decay	$1e^{-2}$	$1e^{-2}$	$1e^{-3}$
Windows	5	1	4
LoRA Learning Rate	$1e^{-2}$	$1e^{-5}$	$1e^{-1}$

A.4. Experiments

In Section A.4, we show the performance of our fine-tuned model LAte and compare it to recent baselines. Here, the EEG common subject variability can be observed, where subject 3 defaults to near random performance while subject 2 achieves almost perfect accuracy. This trend is persistent for all models. However, on previously challenging subjects, e.g., 4 and 5, LAte, with its pretraining and richer subject information, is capable of leveraging features that are shared across the dataset to increase performance.

The hyperparameter search for the learning rate $\{1e^{-3}, 1e^{-4}\}$, weight decay, $\{1e^{-1}, 1e^{-2}, 5e^{-2}, 1e^{-3}\}$, patching windows $\{1,2,3,4\}$ and learning rate of the LoRA weights in the decoder $\{1e^{-1}, 1e^{-3}, 1e^{-5}\}$ was repeated on random seeds and the optimal values selected on the best validation accuracy for MI and SSVEP and the best validation AUC for ERN. The optimal values are shown in Table 6. For CBraMod and TCFormer, we extended the weight decay search grid by adding $1e^{-4}$ as well.